Characterization of GPS Signals in Urban Environments Using Deeply Integrated GPS/IMU

Andrey Soloviev, Dean Bruckner and Frank van Graas
Avionics Engineering Center
Room 231 Stocker Center
Ohio University
Athens, Ohio 45701
USA

soloviev@ohio.edu

ABSTRACT

This research evaluates the quality of GPS signals and their usability for localization in urban environments. GPS signals collected on a Software Defined Radio (SDR) platform in urban canyons in Columbus, Ohio (USA) are processed using a deeply integrated GPS/INS scheme. This architecture allows for coherent signal integration with continuous carrier phase tracking for intervals as long as one second. Results characterize the received signals in terms of signal strength, tracking continuity and multipath influence on signal tracking performance. Results show that signals from 5 to 6 Space Vehicles (SVs) are available for processing, even in dense urban canyons. Deep GPS/INS integration enables continuous carrier phase tracking, thus allowing for accuracies in stationary tests on the cm level in integrated velocity and on the 1 – 2 meter level in relative position. Consistent carrier phase tracking is demonstrated for two or more SVs simultaneously even when all satellite Line of Sight (LOS) vectors are blocked by buildings and Carrier-to-Noise Ratios (CNRs) are as low as 12 dB-Hz. Finally, a photographic method is introduced for visualizing a GPS receiver's "eye view" in an urban canyon.

1.0 INTRODUCTION

Urban environments pose some of the most severe challenges known to developers of Global Navigation Satellite Systems (GNSSs). In the presence of tall and densely packed buildings that block and reflect satellite signals, conventional sequential tracking receiver architectures typically display suboptimal performance. This research attempts to circumvent these limitations by demonstrating an entirely different receiver architecture.

In previous efforts at Ohio University, a real time, Software-Defined Radio (SDR) based, batch processing GPS receiver architecture was developed and tested [1-3]. This architecture was extended to include a low-cost Inertial Measurement Unit (IMU) to perform GPS/IMU deep integration, in order to enable the system to process signals with Carrier-to-Noise Ratios (CNRs) down to 15 dB-Hz [4, 5]. The deep integration mode developed provides consistent carrier phase tracking without requiring the knowledge of navigation data bits. Consistent carrier phase tracking at a 15 dB-Hz level was previously demonstrated in real flight environments [6]. The first characterizations of the availability and quality of GPS signals in urban environments using deeply integrated GPS/IMU were presented in [7]; those results are presented again below and are extended to include more recent analyses.

Soloviev, A.; Bruckner, D.; van Graas, F. (2007) Characterization of GPS Signals in Urban Environments Using Deeply Integrated GPS/IMU. In *Military Capabilities Enabled by Advances in Navigation Sensors* (pp. 17-1 – 17-16). Meeting Proceedings RTO-MP-SET-104, Paper 17. Neuilly-sur-Seine, France: RTO. Available from: http://www.rto.nato.int.

2.0 DATA ACQUISITION ARCHITECTURE AND PROCESSING

The data acquisition system architecture is illustrated in Figures 1 and 2. The system was installed in a Ford Econoline 350 cargo van with roof racks, as shown in Figure 1. Although only one GPS channel was needed for deep integration processing, two channels were available and provided redundancy.

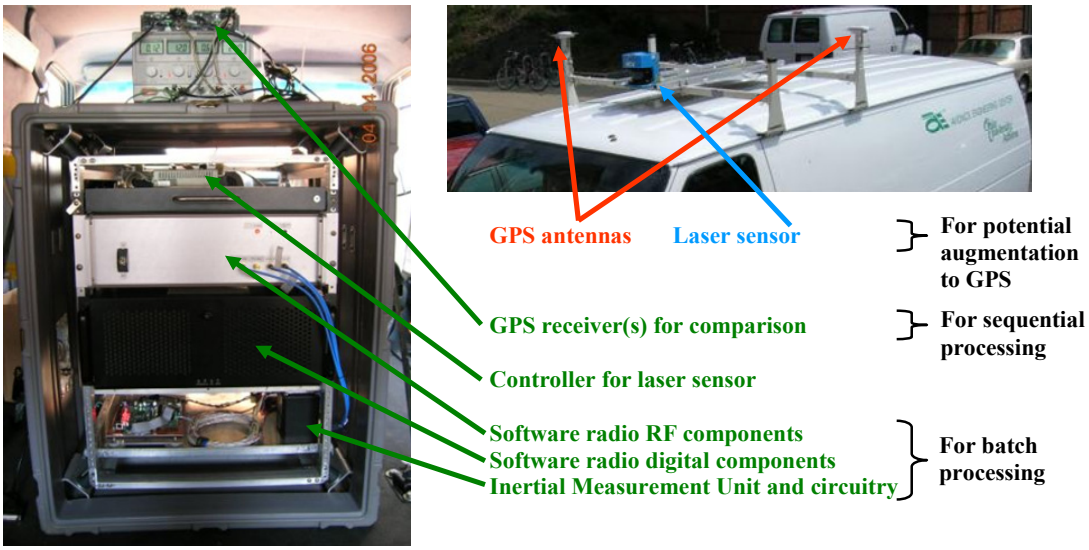

Figure 1: Photographs of Van-Mounted Data Acquisition System

The simplified system block diagram in Figure 2 shows the general data acquisition structure. Two GPS patch antennas, one in the L1 frequency band and the other an L1/L2 active antenna, were present. The first of these antennas provided the signals for deep integration GPS/IMU processing. A SiRF StarIII receiver with its own patch antenna (stated incorrectly in [7] as split from the L1 antenna) was used for comparison. This receiver took the place of the 2 NovAtel OEM-4 receivers shown in the original configuration in Figure 1.

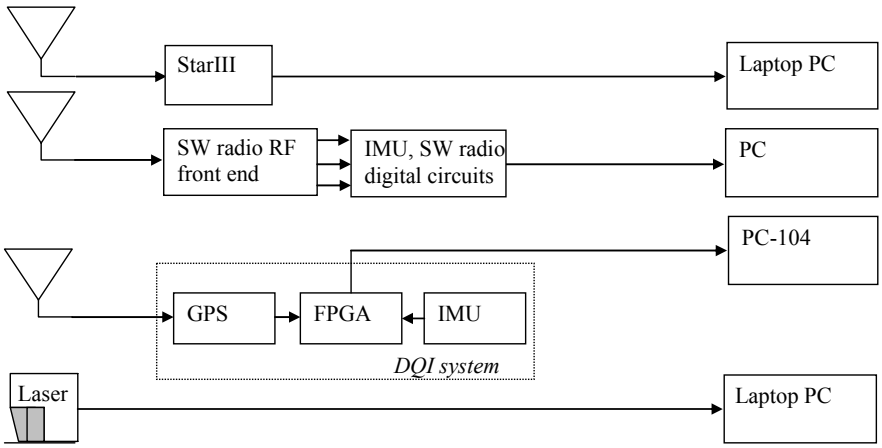

Figure 2: Simplified Data Acquisition Block Diagram

The SDR employs a downconvert-and-digitize front-end [8]. The GPS/IMU deep integration is performed in postprocessing. Details of the downconversion and postprocessing with the American GNC brand IMU are described variously in [2-6] and are not repeated here. The IMU system shown in Figures 1 and 2 consists of a tactical grade Systron Donner Digital Quartz IMU (DQI) sensor, a PC-104 computer controller, Field Programmable Gate Array (FGPA) circuitry and a GPS receiver to time stamp the IMU data [9].

Finally, a Sick brand Laser Measurement Sensor (LMS) 200 provided continuously-panned distance data in a 180-degree arc in the horizontal plane with 0.5 degree resolution [10]. Distance was recorded with cm-level resolution with a maximum range of 80 m. Laser data was manually synchronized to IMU data approximately to the nearest quarter second, and was recorded on a laptop computer.

3.0 RESULTS FOR DEEPLY INTEGRATED GPS/IMU SYSTEM

3.1 Description of Test Area and General Characterization of Signals

The system was tested on the morning of 19 May 2006 in downtown Columbus, Ohio. Columbus is one of the 20 most populous cities in the United States, and contains several areas of urban canyons that represent moderate to difficult challenges for GPS navigation. The photographs in Figure 6 illustrate buildings and structures found in the downtown area. The second photo illustrates two tunnels under pedestrian overpasses on S. Wall Street, each 6 m high and approximately 30 m deep (along the direction of the test vehicle's track).

Figure 3: Downtown Columbus, Ohio (left photo Broad & 4th; right photo S. Wall)

An approximately rectangular test track about 1 mile in length through the downtown area was traversed three times. The comparison receiver, the SiRF StarIII, provided a general characterization of the GPS signals. This receiver reported no less than 5 and no more than 11 visible satellites for the entire test period, but exhibited occasional discontinuities in reported position on the order of 100 m. Errors in reported velocity during certain vehicle stops were at the m/s level. More details of the StarIII performance on this test track are in [7].

3.2 Stationary Tests of the Deeply Integrated GPS/IMU System

Five locations deemed representative of the varied urban densities encountered along the test track were selected for stationary tests of the deeply integrated GPS/IMU system. Stationary tests were chosen for the initial characterization effort to remove all errors in the reference trajectory (i.e., velocity and position are known to be zero). The least challenging of the five scenarios was next to the corner of a tall building but with clear sky views in several directions; the most difficult lay directly under a 30-m long street-level tunnel under a 6-m high pedestrian overpass, with no sky visible at all except for an approximate 10 degree square patch of sky on the horizon to the rear of the vehicle. Fifty to 60 seconds of data were collected in each of the 5 locations, and a 1 s integration interval was applied in postprocessing to maximize signal detection.

Figure 4 shows the urban surroundings for stationary scenario 1, which is approximately at the midpoint of relative difficulty for the five stationary scenarios. The test vehicle stopped for a couple of minutes to obtain the 50 second test interval that appears in subsequent figures. In addition to the forward, or Southeast (SE), view shown in Figure 4, the view to the driver's left (NE) was blocked by a tall building. The view to the passenger's right (SW) was relatively open, while the view to the rear (NW) was largely obstructed by tall buildings. Figures 4 also illustrates the azimuth and elevation of each SV measured, relative to both the north-aligned locally level navigation frame and the Columbus street grid, aligned about ten degrees from north.

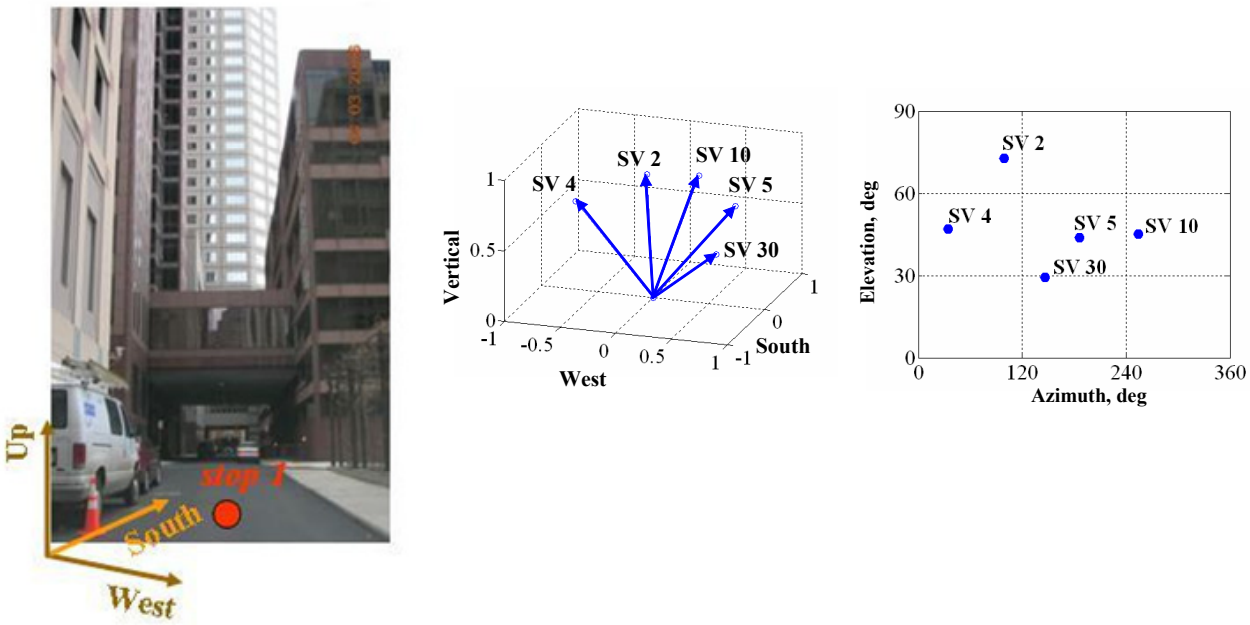

Figure 4: Vehicle Location and Satellite Lines of Sight for Stationary Test Scenario 1

Figure 5 shows 3-D GPS signal images computed by the batch processing algorithm for Space Vehicles (SVs) 4 and 5, which have Carrier to Noise Ratios (CNRs) of 24 dB-Hz and 16 dB-Hz, respectively. The deep integration receiver computes a 3-D image for each signal batch as described in [3] and [4]. The signal is identified when a peak is found.

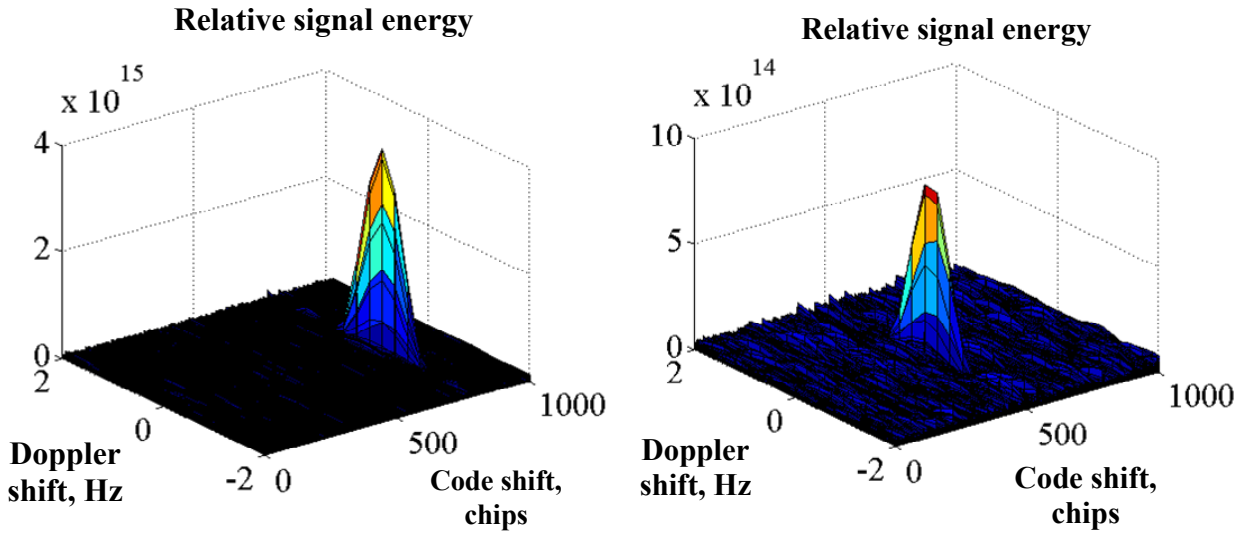

Figure 5: Relative Energy Peaks for SVs 4 (left) and 5 (right), Scenario 1

The quality of GPS signal tracking was assessed in postprocessing in four respects. First, to evaluate availability, the total number of visible SVs for which a signal (either direct path or multipath, or both) was detected and measured was recorded. Second, to evaluate tracking consistency, the carrier phase measurements of each SV were examined for discontinuities. Third, to evaluate tracking accuracy, integrated velocity was derived from the carrier phase measurements as described in [11] and compared to the true vehicle velocity, which was zero. Fourth and finally, the change in position of the vehicle over the test interval, derived from the velocity, was computed and compared to the true change in position, which was also zero.

To support this type of analysis, the deep integration receiver measures accumulated Doppler and CNR, as illustrated in Figure 6. The term δ (Accumulated Doppler) is used herein to denote accumulated Doppler measurements that are compensated for the satellite motion component, as well as receiver clock, ionospheric and tropospheric first-order drift components. The satellite motion component is computed from ephemeris data as described in [11]. Polynomial approximation is applied to compensate for the first-order drift terms.

Figure 6 demonstrates consistent carrier phase tracking. In other words, successive accumulated Doppler measurements do not exhibit discontinuities. As the SVs move in relation to the stationary test van and downtown buildings, gradual changes are seen in both the carrier phase measurement and the CNR. For the 1 s integration intervals used in these tests, a measured CNR of approximately 12 dB-Hz marked the threshold below which carrier phase tracking became inconsistent. Of the five SVs tracked in this scenario, plots from SVs 4 and 5 were shown in [7] while plots from SVs 2 and 30 appear here. Plots from SV 10 appear in both.

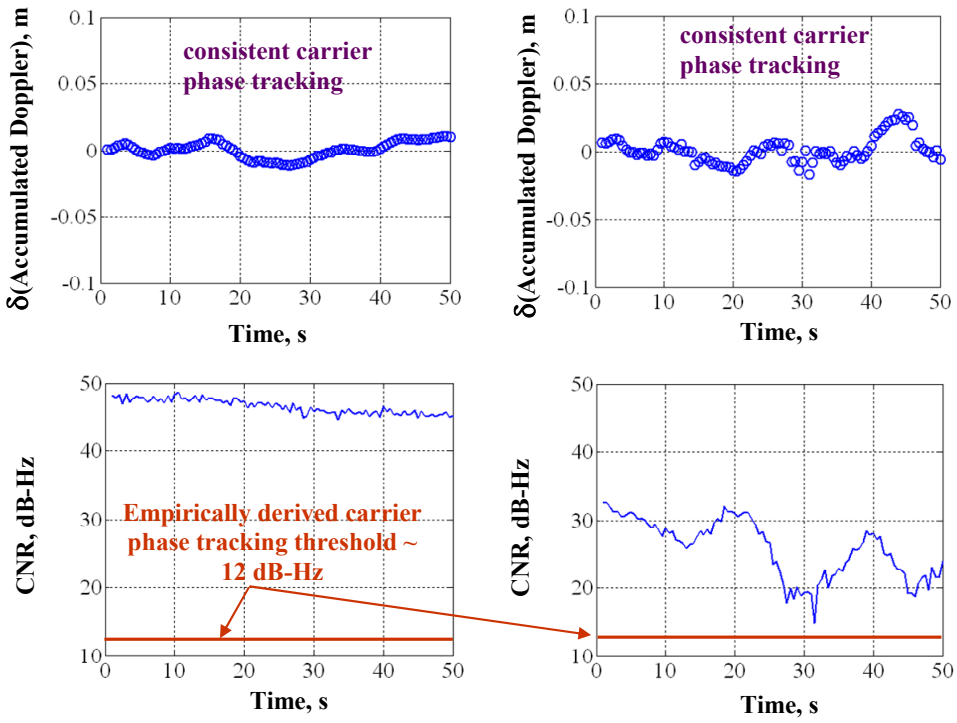

Figure 6: Accumulated Doppler and CNR for SVs 2 (left) and 30 (right), Scenario 1

From subsequent examination of the city street and surrounding buildings, as well as the plots above, it is apparent that SV 2 is a direct path signal, while SV 30 is an indirect path signal. Nonetheless, signals from both SVs exhibit consistent carrier phase tracking for the entire 50-second length of the stationary test scenario.

Several interesting effects are seen in Figure 7, which displays parameters for SV 10 in scenario 1. As the SV moves in relation to the stationary test van and buildings, some of the multipath signals add destructively to the direct path, or to each other. This effect reduces CNR to a level below the empirically-identified tracking threshold. Figure 7 shows two carrier phase discontinuities, one for each of two episodes of multipath fading that occur approximately 14 seconds apart. When the receiver tracking function recovers, a discontinuity of 9 to 10 cm appears in the accumulated Doppler.

Code phase tracking performance is similarly affected by multipath fading, which is also shown in Figure 6. At these instants, the phase adjustment exceeds the correlator spacing, and the code phase adjustment applied by the deep integration receiver exhibits considerable fluctuations. Similarly, the code minus carrier calculation displays a similar fluctuation. The open-loop, batch processing architecture allows the code-phase tracking to resume within one signal accumulation interval, which is 1 s, after the fading disappears.

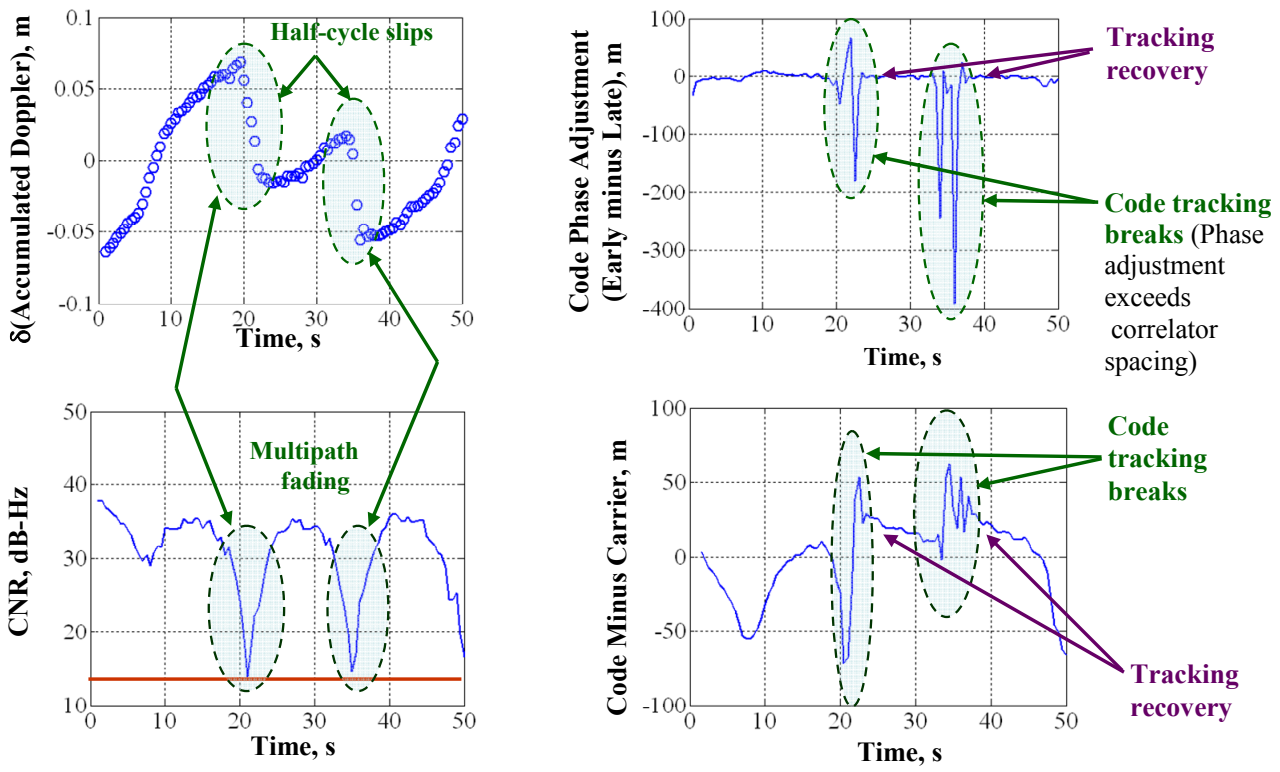

Figure 7: Carrier Phase, CNR and Code Phase Anomalies due to Signal Fading for SV 10, Scenario 1

The left portion of Figure 8 shows performance of the receiver integrated velocity computed from carrier phase measurements for Scenario 1. The integrated velocity herein is defined as a receiver velocity integrated over the carrier phase update interval, in this case 1 s. Integrated velocity, with units of distance, is preferable to velocity in this application because it provides the best indication of the noise level in the carrier phase measurements by remaining independent of the integration time interval. Details of the integrated velocity computations can be found in [11]. The integrated velocity measurements in Scenario 1, derived from carrier phase measurements of up to five SVs, show consistent cm-level performance with standard deviations of 0.65 cm, 0.81 cm and 1.39 cm respectively in the north, east and up directions.

The change in user position reported by the deeply integrated receiver appears on the right portion of Figure 8. This quantity is computed identically to the integrated velocity, but over the entire 50 s test interval instead of the 1 s aiding interval. The error in position at the end of the 50 s test interval, relative to the position at the beginning of the test interval, is on the 1-2 meter level.

Errors in the user's initial position are transformed into relative position errors through geometry compensations of the type described in [11], in which the user's position is an argument in the calculations performed. For a 50 m initial position error, vertical relative position errors on the order of 1-2 m are seen by the end of the 50 s test interval. Multipath errors can also contribute to the relative position error. Movements in the receiver or satellite relative to the reflecting plane contribute to a line of sight (LOS) velocity difference between the direct path and multipath signals. For reflecting planes within 100 m of the receiver, the magnitude of this difference in integrated velocity is less than 1 cm, translating to a vertical relative position

bias on the order of 0.8 to 1.2 m by the end of the 50 s test interval in Scenario 1. The combined vertical error from these two error sources is on the order of 2-3 m by the end of the test interval.

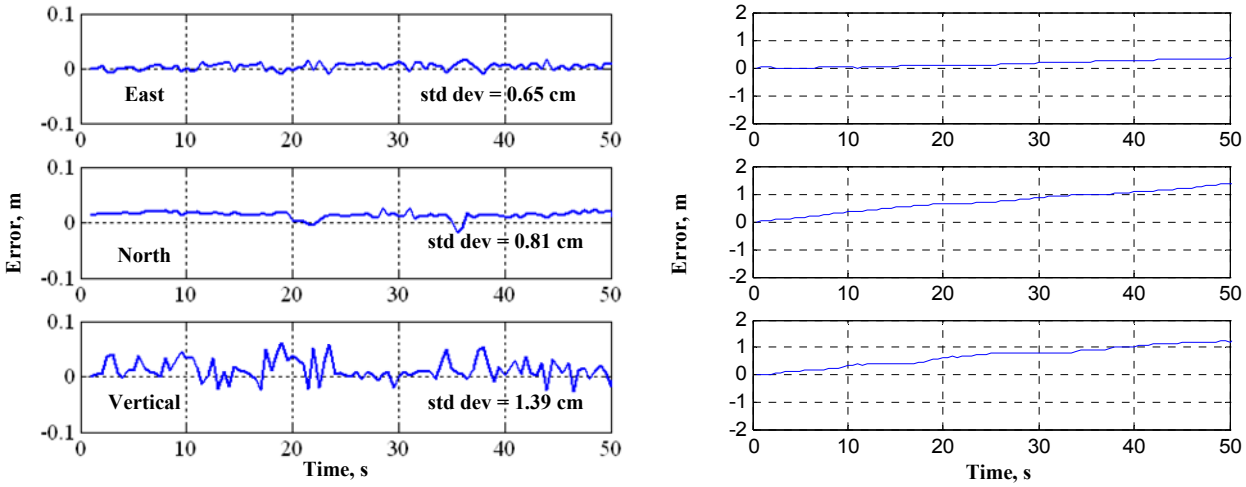

Figure 8: Integrated Velocity Performance (left) and Relative Position Performance (right), Scenario1

Table 1 summarizes the results of the stationary tests for all five scenarios, shown in order from most to least challenging. From this data, it is apparent that direct or indirect path signals from 5 to 6 SVs are available for processing in dense urban canyons, including scenarios where no direct path signals exist. Centimeter-level accuracies in carrier phase-based integrated velocity are obtained in all scenarios, even in the case where no direct path signals exist. Millimeter-level accuracies in integrated velocity are obtained in some scenarios. Finally, consistent carrier phase tracking is demonstrated for at least 2 SVs in the most difficult scenario (no direct path signals) and for up to 5 SVs in less challenging scenarios.

Table 1: Results of Stationary Tests: Carrier Phase (CP) Parameters

Scenario number	**2**	**3**	**1**	**4**	**5**
Relative difficulty (hardest to easiest)	5	4	3	2	1
Accuracy level of CP-based integrated velocity:	cm	mm	cm	cm	mm
• **Integrated velocity error sigma in East direction (cm)**	1.38	0.55	0.65	0.88	0.24
• **Integrated velocity error sigma in North direction (cm)**	0.84	0.48	0.81	0.28	0.44
• **Integrated velocity error sigma in Vertical direction (cm)**	2.59	0.90	1.39	1.14	0.49
Num of SV channels with consistent CP tracking	2	3	4	5	5

3.3 Dynamic Tests of the Deeply Integrated GPS/IMU System

Examination of the instantaneous frequency of multipath signals in a moving test vehicle reveals that significant differences from the instantaneous frequency of the direct path signal can exist. These differences exist for those cases where LOS vectors from the SV to the receiver, and from the reflecting object to the receiver, differ significantly from each other, and the projection of the receiver velocity on the LOS vector from the reflecting object is non-zero. The vector difference between the two components of the receiver velocity along these two directions is $|\Delta \mathbf{V}|$, as shown in Figure 9 below. When postprocessed in the deep integration receiver by computing 3D signal images, also shown in Figure 9, the direct path signal energy peak is readily distinguishable from the multipath signal peak(s). Further research will exploit this phenomenon.

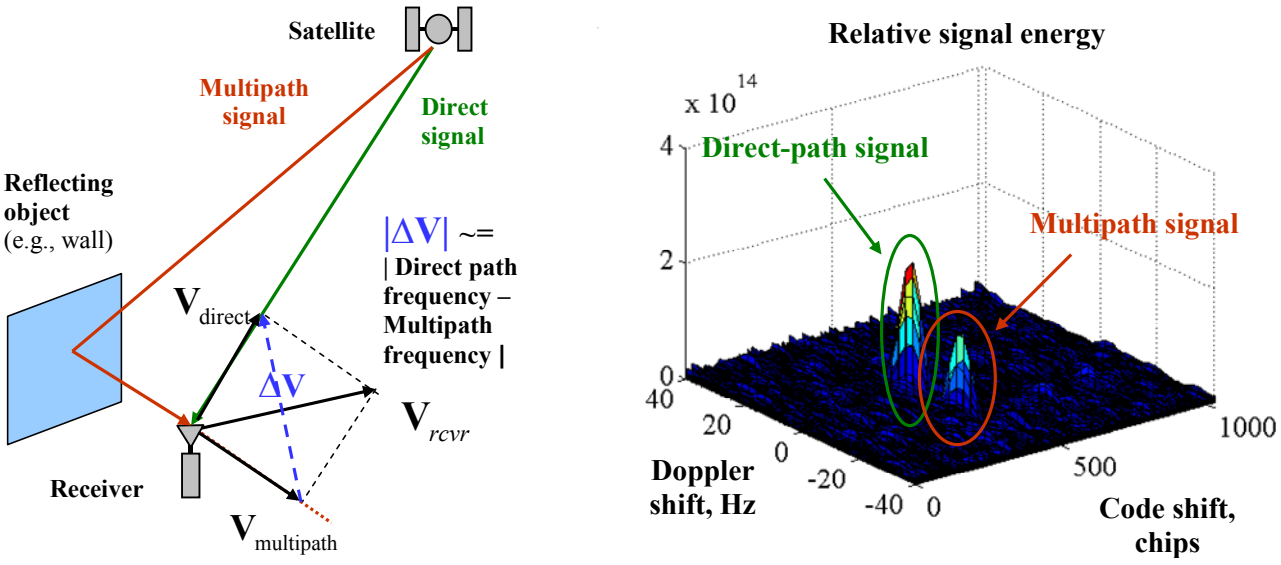

Figure 9: Differences between Direct and Multipath Signals for Non-zero Receiver Velocity

4.0 SIMULATED INTEGRATION WITH LOW-GRADE IMU

For designs that move beyond the prototyping stage, a critically important design aspect is the relationship between IMU cost and overall system performance, here exemplified by consistent carrier phase tracking. To establish an empirical relationship between these two criteria, a simulation was performed as follows:

- Three IMU sensor performance models were created to span the performance space between the DQI (approximately $15,000 when purchased in 2005) on one end and IMUs expected to be available in the next few years in the $1,000 range on the other end. These were designated Low Grade IMU 1, 2 and 3, as shown in Table 2.
- Inertial sensor data obtained from the DQI was corrupted with accelerometer biases and gyroscope drifts. Inertial sensor errors were simulated as first-order Gauss-Markov processes with a time constant of 100 s.

- The maximum allowable deep GPS/IMU integration period for each sensor performance model was determined by identifying when the 3-sigma INS error, mapped into the position error space, exceeded one quarter wavelength of the GPS L1 carrier frequency, as shown in Table 2 and Figure 10 below.
- The reduced integration times and CNRs for each sensor performance model were applied to the five stationary cases presented above, and overall system performance was determined in postprocessing.

Table 2: Simulated IMU Sensor Performance Models

Model characteristics	Low Grade IMU 1	Low Grade IMU 2	Low Grade IMU 3
Estimated cost	$4,000	$2,000	<$1,000
Maximum integration interval (s)	1	0.72	0.46

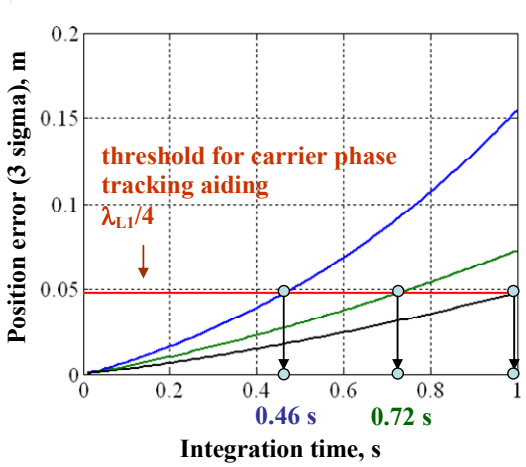

Figure 10: Simulated Error Growth for 3 IMU Sensor Performance Models

Table 3 below shows the number of SVs that would have been visible in the five stationary tests with IMUs of these varying simulated performance characteristics. The 12 dB-Hz signal processing threshold used previously is increased for each IMU model by amounts corresponding to the decreased allowable integration times shown in Figure 10 above. Table 3 also reveals that the number of SVs visible is fairly insensitive to reductions in IMU quality. Scenario 2, the most difficult of all the stationary scenarios, is the only one to show any reduction in SVs visible as a result of simulated IMU performance reductions.

Table 3: Performance of IMU Sensor Models

IMU Grade	Number of SVs Visible					# of SV Channels with Consistent Carrier Phase Tracking				
Scenario number	*2*	*3*	*1*	*4*	*5*	*2*	*3*	*1*	*4*	*5*
Relative difficulty	*5*	*4*	*3*	*2*	*1*	*5*	*4*	*3*	*2*	*1*
DQI	5	6	5	5	6	2	3	4	5	5
Low Grade IMU 1	5	6	5	5	6	2	3	4	5	5
Low Grade IMU 2	5	6	5	5	6	1	2	3	4	5
Low Grade IMU 3	3	6	5	5	6	0	2	3	4	5

Also shown in Table 3 is the number of SV channels displaying consistent carrier phase tracking for each of the IMU sensor models. The variation of the number of SV channels with consistent carrier phase tracking with both IMU grade and difficulty of scenario are better understood with the aid of the graph that appears in Figure 11. IMU cost is seen to be more correlated to the number of channels with consistent carrier phase tracking (and hence to overall system performance) than to the number of SVs visible. IMU performance levels better than those with a nominal cost of $4,000 per unit yield no apparent improvement in overall system performance. IMU performance levels worse than this level yield an almost linear reduction in overall system performance down to zero consistent carrier phase tracking channels in the most difficult scenario.

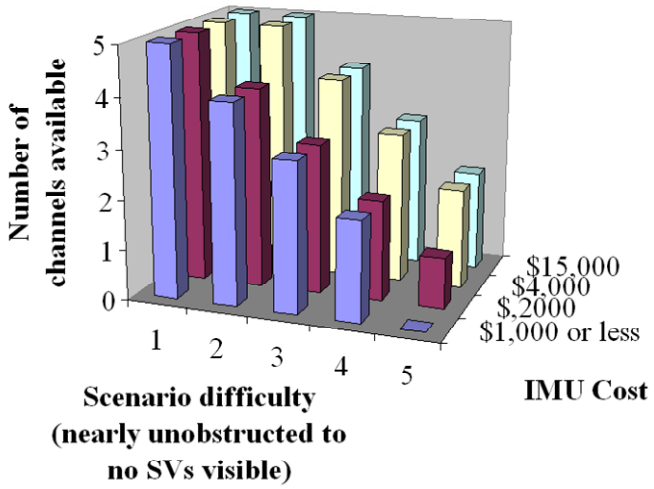

Figure 11: Number of SV Channels with Consistent Carrier Phase Tracking

5.0 PHOTOGRAPHIC VISUALIZATION OF GPS RECEIVER ENVIRONMENT

The confusing overlay of direct path and multipath GPS signals in urban canyons presents a difficult challenge to analysis. This difficulty arises in part from the highly varied collection of solid shapes that block satellite signals and complex surface features that reflect, diffract and attenuate these signals. Photographs of particular urban canyons can be helpful in recording details for postprocessing and analysis, but the limited field of view in typical photographic images is of limited value in illustrating how these structures act upon the satellite signals from the point of view of a receiver.

"Fish-eye" photographic images result from using optical lenses with very short focal lengths—on the order of 8 mm for a 35mm format camera as opposed to the typical wide angle lens focal lengths of 20 – 35 mm. Fish-eye images provide distinct advantages for visualization and analysis of GPS signal behavior in urban canyons. When pointed directly up, a camera with a fish-eye lens records essentially a receiver's eye view of the sky, including all obstructions between the receiver and satellite all surfaces that may reflect and diffract the signal. Because the image is also essentially a circular representation of a hemisphere (i.e., a polar azimuthal cartographic projection), the azimuth and elevation angle of each satellite may be plotted on the image, readily showing obstructions between the satellite and receiver. Furthermore, these images directly illustrate the most important feature of urban areas to satellite navigation: the portion of sky visible.

A low cost ($70 USD) 35mm format fish-eye camera with an effective focal length of approximately 8 mm was used to obtain sky-view images of the urban canyons of Columbus, Ohio. The viewable portion of the images from this camera spans approximately 130 degrees in the wider dimension and 100 degrees in the narrower dimension, sufficient to capture virtually the entire portion of the sky visible above 30 degrees elevation from the horizon. Six-megapixel JPEG digital images were obtained from the film negatives using standard commercial photo processing. Although a commercially available, professional quality full-frame 35 mm digital camera and 8 mm lens would provide virtually circular 180-degree images in both still and movie format, the cost (in excess of $2,000 USD) was deemed excessive for this proof of concept. In addition, most of the sky visible from the horizon to 30 degrees elevation is typically blocked in urban canyons.

The left image of Figure 12 shows a sample fish-eye image of an urban canyon 5 m wide and with walls approximately 12 - 15 m high. The gray ring visible is the lens rim. The right image shows the portion of sky, here computed as 32%, recognized by a digital image processing algorithm written by the authors. This algorithm compares the RGB color values of each pixel to each of eight different sample sky pixels selected by the user, and applies a threshold. If the pixel matches the color of any of the eight samples, it is classified as being sky. The pixels are weighted to adjust for lens distortion near the edges (i.e., compression of the elevation dimension). The percent of sky visible above 30 degrees elevation is then computed as a simple figure of merit for the suitability of the location for GPS reception. Note that portions of two building walls reflecting strong sunlight are incorrectly classified as sky. The error of this method is approximately ± 5%.

A set of 90 images was taken at approximate 20 m intervals along the 1-mile long, roughly rectangular GPS test track used in Columbus, Ohio. The percent of sky visible was computed for each image, and a color code was assigned to each value—red for less than 20 percent sky visible above 30 degrees, green for more than 80 percent, and yellow for values in between—with interpolation applied between these colors. In green areas, any GPS receiver is expected to operate successfully. In yellow areas, receivers optimized for urban use, such as the SiRF StarIII, are expected to work reasonably well. In red areas, few existing receivers are expected to work. Figure 13 shows the percent of sky visible along this track. Figure 13 shows the percent of sky visible along this track, a simple metric that describes the extent to which a receiver's view is obstructed.

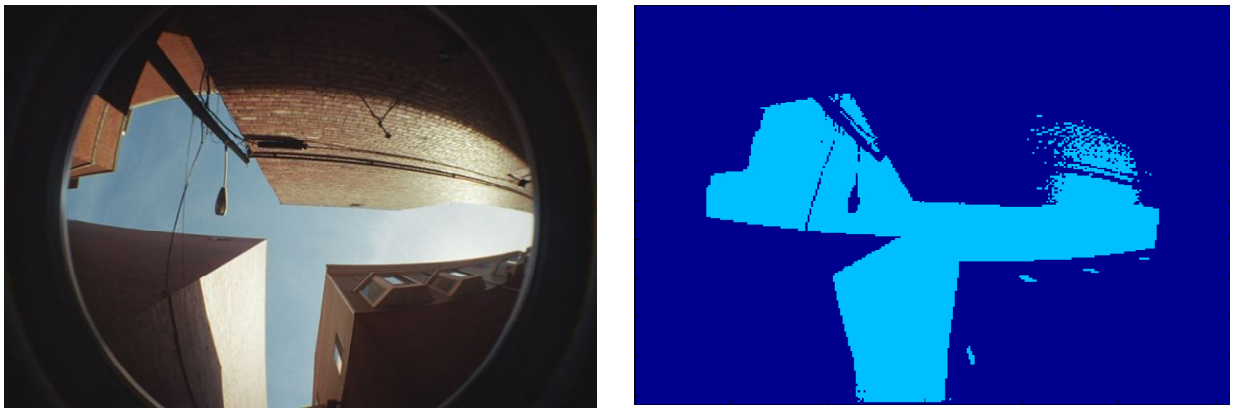

Figure 12: Sample Fish-eye Image (left) and Image Pixels Recognized as Sky (right)

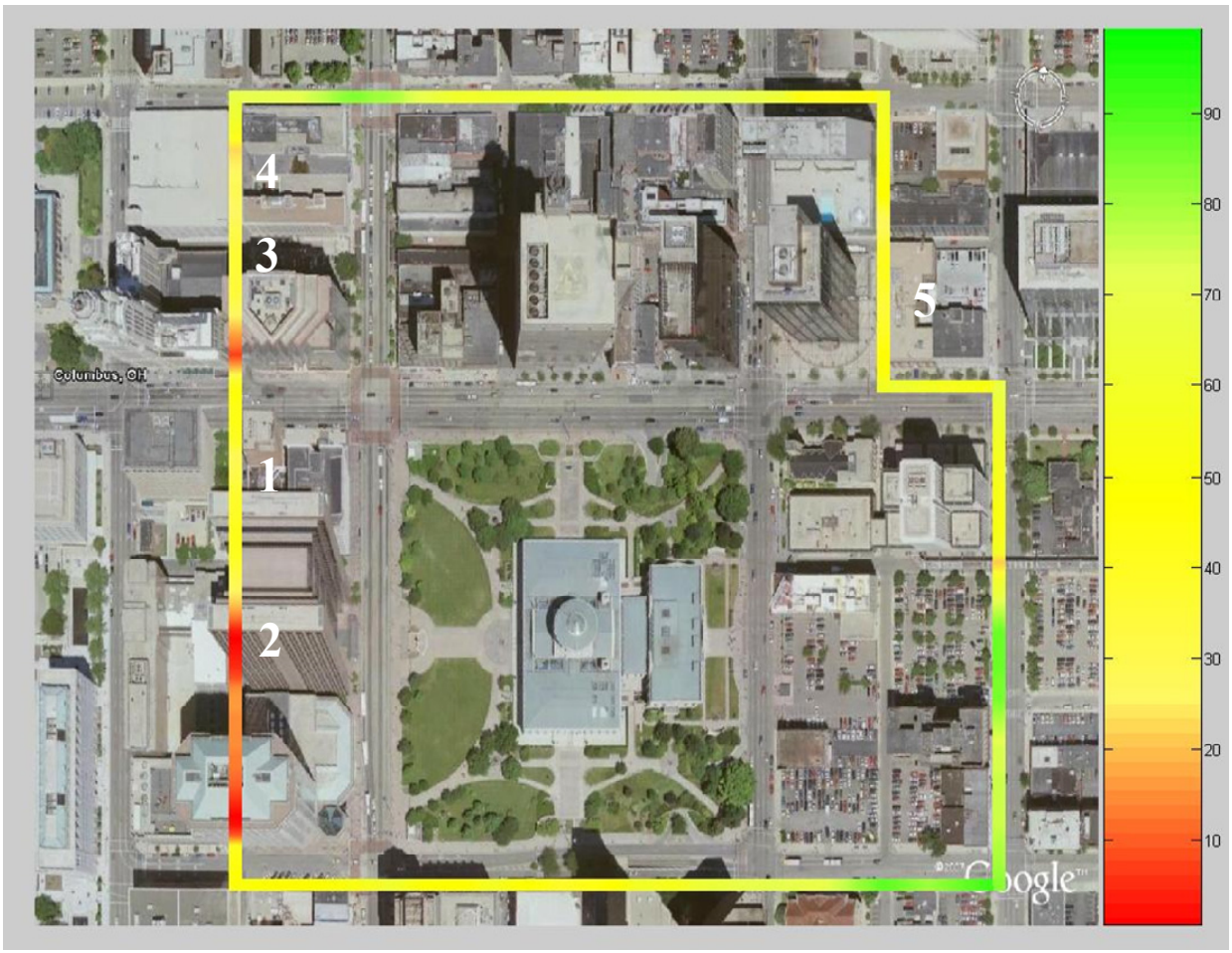

Figure 13: Percent of Sky Visible on Test Track, Columbus, Ohio (0 – 100% as shown by color bar), with Stationary Test Locations Indicated

Figure 14 shows the overlay of the 5 satellites tracked in stationary test Scenario 1, superimposed over a fish-eye image of the sky view above the test location. The CNR values from 45 to 48 dB-Hz (for 1 s integration time) for SV 2 confirmed that this signal was direct path, while CNR values uniformly below 35 dB-Hz for SVs 4, 5 and 30 indicate that those signals were indirect paths only. The signal from SV 10 evidences fading, likely between the direct and indirect paths. An estimated 28% of sky above 30 degrees elevation is visible from this location.

Figure 14: Approximate Satellite Locations for Stationary Scenario 1

The satellite icons shown with '*' are those for which consistent carrier phase tracking was achieved for the entire 50-second test interval. In this and all of the other stationary scenarios, there seems to be no detectable pattern to which SV signals were tracked with continuous carrier phase. In all likelihood, the three dimensional spatial pattern of signals with continuous carrier phase is highly variable in space and slowly varying in time.

The metric of percent of sky visible obviously does not take into account the blocking and reflecting of individual satellite signals at a particular GPS epoch. Therefore, this metric cannot predict the performance level of the deeply integrated GPS/IMU receiver beyond the general red-yellow-green classification already discussed.

6.0 CONCLUSIONS

GPS signals in urban canyons are characterized as they appear to a deeply integrated GPS/IMU receiver with an open-loop tracking architecture. Signals from 5 to 6 SVs are available for processing by the deeply integrated GPS/IMU receiver even in very dense urban canyons. The quality of these signals for tracking purposes is assessed in four respects. First, carrier phase-based integrated velocity is shown to be accurate at least to cm level in all scenarios, and to mm level in some scenarios. Second, relative position is shown to be accurate to within 2 – 3 m for 50 to 60 second test intervals. Third, consistent carrier phase tracking is demonstrated for at least 2 SVs in the most challenging scenario, where no direct path signals exists, and up to 5 SVs in less difficult scenarios. Fourth, signal tracking can break down when CNR is below 12 dB-Hz (corresponding to a 1 s integration interval), or due to multipath fading.

The difference in frequency between direct path and multipath GPS signals is shown to provide a clear way to distinguish between these signals. Frequency is thus a potentially useful factor for identifying and tracking GPS signals in dynamic scenarios.

The relationship of cost versus performance for IMU quality in a deeply integrated GPS/IMU architecture is shown to be a fairly smooth slope, within bounds. The limiting performance factor appears to be the number of channels with consistent carrier phase tracking. The range of interest in IMU unit estimated cost is from less than $1,000 upwards to an expected $4,000. In the most difficult scenario, where no direct path SV signals are received, the improvement in overall system performance increases nearly linearly with increased cost.

Fish-eye images are useful for visualization and analysis of GPS signals in urban canyons. The metric of percent sky visible, however, is of limited use for predicting performance of a deeply integrated GPS/IMU receiver. A more useful metric would better account for signal complexity by predicting SV blockages from buildings, predicting the location and strength of multipath signals and the resulting degradation to direct path signals, and predicting both multipath fading and low CNR conditions. Such a metric might yield predictions of which SVs would exhibit continuous carrier phase. This would require data sources that describe reflecting surfaces, possibly from databases of buildings and/or active imaging systems such as radar or lidar. If used together, such data sources may become more effective than GNSS systems for urban use and may thus quickly bypass a supporting role altogether.

7.0 ACKNOWLEDGEMENTS

This paper is based on one previously presented in January 2007 at the Institute of Navigation's National Technical Meeting in San Diego, California.

The Robert Bosch Corporation, RTC funded portions of this research. The Federal Aviation Administration also funded prior research into frequency multipath effects, which was important to this research.

8.0 REFERENCES

[1] Marti, L. *The Effects of the Radio Frequency Front-End Onto Signal Estimation*. Proceedings of the Institute of Navigation GPS-2003, 9-12 September 2003, Portland, OR, USA.

[2] Gunawardena, S., van Graas, F. and Soloviev, A. *Real Time Block Processing Engine for Software GNSS Receivers*. Proceedings of the ION NTM, 26-28 January 2004, pp. 371-377, San Diego, CA, USA.

[3] van Graas, F., Soloviev, A., Uijt de Haag, M., Gunawardena, S. and Braasch, M. *Comparison of Two Approaches for GNSS Receiver Algorithms: Batch Processing and Sequential Processing Considerations*. Proceedings of the ION GNSS-2005, 13-16 September 2005, Long Beach, CA, USA.

[4] Soloviev, A., van Graas, F. and Gunawardena, S. *Implementation of Deeply Integrated GPS/Low-Cost IMU for Reacquisition and Tracking of Low CNR GPS Signals*. Proceedings of the ION NTM, 26-28 January 2004, San Diego, CA, USA.

[5] Gunawardena, S., Soloviev, A. and van Graas, F. *Real Time Implementation of Deeply Integrated Software GPS Receiver and Low Cost IMU for Processing Low-CNR GPS Signals*. Proceedings of the ION 60th Annual Meeting, 7-9 June 2004, Dayton, OH, USA.

[6] Soloviev, A., Gunawardena, S. and van Graas, F. *Deeply Integrated GPS/Low-Cost IMU for Low CNR Signal Processing: Flight Test Results and Real Time Implementation*. Proceedings of the ION GNSS-2005, 13-16 September 2005, Long Beach, CA, USA.

[7] Soloviev, A., Bruckner, D. and van Graas, F. *Assessment of GPS Signal Quality in Urban Environments Using Deeply Integrated GPS/IMU*. Proceedings of the ION NTM, 22-24 January 2007, San Diego, CA, USA.

[8] Tsui, J. B. *Fundamentals of Global Positioning System Receivers: A Software Approach*. New York: John Wiley & Sons, Inc., 2000.

[9] Data sheet for DQI-digital quartz IMU (www.systron.com/PDFS/datasheets/DQI.pdf)

[10] *Technical Description of the LMS 200, LMS 220, LMS 211, LMS 221, LMS 291 Laser Measurement Systems*. Revised June 2003 (www.mysick.com/saqqara/pdf.aspx?id=im0012759)

[11] van Graas, F. and Soloviev, *A. Precise Velocity Estimation Using a Stand-alone GPS Receiver*. Proceedings of the ION NTM, January 22-24, 2003, Anaheim, CA, USA.

[12] GPS Chip Solution: SiRF StarIII GSC3e/LP (www.sirf.com/products/gps_chip.html)